An Evaluation of the Uncertainty of the GSICS SEVIRI-IASI Intercalibration Products

Tim J. Hewison, *Senior Member, IEEE*

***Abstract*—Global Space-based Inter-Calibration System (GSICS) products to correct the calibration of the infrared channels of the Meteosat/SEVIRI (Spinning Enhanced Visible and Infrared Imager) geostationary imagers are based on comparisons of collocated observations with Metop/IASI (Infrared Atmospheric Sounding Interferometer) as a reference instrument. Each step of the cross-calibration algorithm is analyzed to produce a comprehensive error budget, following the Guide to the Expression of Uncertainty in Measurement. This paper aims to validate the quality indicators provided as uncertainty estimates with the GSICS correction. The methodology presented provides a framework to allow quantitative tradeoffs between the collocation criteria and the number of collocations generated to recommend further algorithm improvements. It is shown that random errors dominate systematic ones and that combined standard uncertainties (with coverage factor $k = 1$) in the corrected brightness temperatures are ∼0.01 K for typical clear sky conditions but increase rapidly for low radiances—by more than one order of magnitude for 210 K scenes, corresponding to cold cloud tops.**

***Index Terms*—Calibration, Earth Observing System, infrared (IR) image sensors, measurement uncertainty, meteorology.**

I. Introduction

TRACEABILITY is one of the key principles of the Global Space-based Inter-Calibration System (GSICS) [1]. Ensuring traceability of its products to a common reference relies on conducting an unbroken chain of comparisons, each with a stated uncertainty. With that intention, this paper reviews the uncertainties introduced at each step of the intercalibration algorithm used to generate *GSICS corrections* for the infrared (IR) channels of the geostationary (GEO) Meteosat/Spinning Enhanced Visible and Infrared Imager (SEVIRI) imager using the low Earth orbit (LEO) Metop/Infrared Atmospheric Sounding Interferometer (IASI) as a reference instrument. These *GSICS corrections* are functions which transform the observations' calibration to be consistent with that of the common reference. These are examples of GSICS products in the GEO–LEO IR class.

A similar analysis was recently presented for a limited number of factors, determined to be dominant, in the cross-calibration of Landsat-7/ETM+ (Enhanced Thematic Mapper Plus) with Terra/MODIS (Moderate Resolution Imaging Spectroradiometer) [2]. Similar techniques have also been used to analyze the MODIS IR channels' calibration by assessing the impacts of onboard radiance uncertainties and combining these in an error budget [3].

The intercalibration algorithm is based on the selection of observations from the GEO *monitored instrument* and the LEO *reference instrument* that are collocated in space, time, and viewing geometry [4], [5]. The collocated observations are transformed to be comparable on spatial scales and spectral coverage and compared using a weighted regression. Each pair of collocated observations is allocated a weight based on its measured spatial variance and the specified radiometric noise of each channel. The regression propagates these variances to estimate the uncertainty on the corrected radiance, which is provided as a *quality indicator* for the intercalibration product.

II. General Principles

In this analysis, uncertainties are analyzed through a *measurement model* of the algorithm's processes, as described in the Algorithm Theoretical Basis Document (ATBD) [6]. Each process is considered, and the uncertainties that it introduces to each collocated radiance are evaluated due to random and systematic effects. These uncertainties are then combined to produce an error budget giving a *Type B* evaluation [7] of the uncertainty on the intercalibration bias. The random component of this is then compared to the statistics of time series of results from the intercalibration algorithm. Based on this, recommendations can be made for adjustments of the intercalibration algorithm to produce more consistent uncertainty estimates. This analysis follows the guidance provided by QA4EO [8], which is based on the Guide to the Expression of Uncertainty in Measurement [7].

For each process of the intercalibration algorithm, typical differences in sampling variables between the monitored and reference instruments are estimated—either from the specified limits used to select the collocations (e.g., spatial sampling) or from the known differences (e.g., in sampling time). These differences are referred to as Δx in this paper. The sensitivity $\partial L/\partial x$ of the radiances in each collocation to perturbations in each variable is also estimated.

The quantities input to the intercalibration process are the radiances L of each collocation i. In general, the standard uncertainty (i.e., with a coverage factor $k = 1$) on L_i due to process j is

$$u_j(L_i) = \Delta x_{i,j} \left(\frac{\partial L}{\partial x} \right)_j . \quad (1)$$

Manuscript received February 13, 2012; revised July 31, 2012 and October 31, 2012; accepted November 20, 2012. Date of publication February 5, 2013; date of current version February 21, 2013.

The author is with the European Organisation for the Exploitation of Meteorological Satellites, 64295 Darmstadt, Germany (e-mail: tim.hewison@eumetsat.int).

Color versions of one or more of the figures in this paper are available online at http://ieeexplore.ieee.org.

Digital Object Identifier 10.1109/TGRS.2012.2236330

TABLE I
SUMMARY OF THE SYSTEMATIC ERRORS' PERTURBATIONS AND SENSITIVITIES TO EACH COLLOCATED RADIANCE

Systematic Error Type	Δx_j^s		*Sensitivity, $\partial L_j/\partial x^s$ [$\mu W/m^2/sr/cm^{-1}/\Delta x$]*							
			IR3.9	IR6.2	IR7.3	IR8.7	IR9.7	IR10.8	IR12.0	IR13.4
Temporal Mismatch	30	s	-0.002	-0.011	-0.014	-0.019	-0.023	-0.141	-0.124	-0.152
Longitudinal Mismatch	1.306	km	-0.010	0.080	0.020	-0.480	-0.260	-0.630	-0.520	-0.170
Latitudinal Mismatch	1.306	km	0.030	0.070	0.320	1.410	0.900	1.920	2.000	1.290
Geometric Mismatch	-0.00069		0. 49	8.6	30.6	34.6	109.9	37.4	47.8	112.8
Spectral Mismatch	1		0.14	0.00	0.00	0.00	0.00	0.00	0.00	0.00
Spectral Calibration	2	ppm	0.09	0.2	0.3	0.2	0.3	0.1	0.1	0.4

The *GSICS Correction*, $g(L)$ is based on the regression of collocated radiances observed by the monitored and reference instruments [4]. As described in [4, Section II-H], all collocations within a window period of the applicable date are combined in this regression. This period is defined as ± 14 days for the *reanalysis corrections* of SEVIRI and $-14/+0$ days for the *near-real-time corrections* and was selected to ensure negligible drift in the instrument calibration [6]. These GSICS corrections are functions which convert radiances observed by the monitored instrument L to be consistent with the calibration of the reference $\hat{L}$

$$\hat{L} = g(L). \tag{2}$$

In this analysis, the observed radiances of each collocation L_i are perturbed by $u(L_i)$. Then, the regression is recalculated to generate a modified function $g'(L)$, which will produce different corrected radiances $\hat{L}'$

$$\hat{L}' = g'\left(L_i + u(L_i)\right). \tag{3}$$

This quantifies how errors in the collocated radiances can be propagated through to errors in the GSICS correction applied to different scene radiances. These provide estimates of the uncertainty on the GSICS correction, which are converted into brightness temperatures using the derivative of the Planck function evaluated over a range of scene radiances.

The uncertainties due to various mechanisms introducing systematic and random errors are analyzed in the following sections, based on case studies, which were selected so that the range of radiances covers most of the dynamic range observed by SEVIRI (at least at night). This is important to prevent extrapolation errors. Repeated evaluations with other cases have shown that the results of the combined uncertainty vary by $\sim \pm 20\%$, depending on the distribution of collocated radiances used as input to the calculation of the GSICS correction. However, the variability of the evaluation of individual terms is much greater than this. Together, these limit the accuracy of this uncertainty analysis to a factor of approximately two.

III. SYSTEMATIC ERRORS

Although the collocation algorithm was designed to ensure that samples are symmetrically distributed, in reality, small residual differences remain, which introduce systematic errors in the end products. These sampling differences introduce errors in the radiances of each collocation, depending on their sensitivity to each variable, which is estimated using statistics from case studies. Where information is available on the sampling distribution, this has been used in the analysis—otherwise, the collocation criteria have been taken as limits and propagated as standard uncertainties assuming that the errors follow rectangular distributions within these limits. These are relatively simplistic treatments, which could be revised for the dominant terms if more accurate analysis were deemed necessary, following the approach recommended by ISO 14253-2: 2011 [9], which defines this iterative procedure for uncertainty management [10].

A. Methodology for Systematic Errors

For each process j introducing systematic errors, the radiance of each collocated point is perturbed by an amount representing its estimated uncertainty $u_j^s(L_i)$ following (1)

$$u_j^s(L_i) = \Delta x_{i,j}^s \left(\frac{\partial L}{\partial x^s}\right)_j. \tag{4}$$

Table I summarizes the magnitude of typical perturbations Δx_j of processes introducing systematic errors in the collocated radiances and the sensitivity of the IR channels of SEVIRI to these perturbations $\partial L/\partial x^s$. The origins of these values are discussed in the following sections.

The regression used to calculate the GSICS correction is recalculated, giving a modified function $g^s(L)$. This function is evaluated for a range of scene radiances, and the resulting radiances are compared to the corrected radiances generated by the unmodified function $g(L)$ to provide an estimate of the uncertainty on the corrected radiance due to systematic errors introduced by process j, which are shown in Fig. 1

$$u_j^s(\hat{L}) = \left|g_j^s(L) - g_j(L)\right|. \tag{5}$$

B. Temporal Mismatch

Systematic differences in the sampling time of the monitored and reference instruments can introduce systematic errors in their collocated radiances due to the diurnal cycle in the temperature, humidity, cloud, and, hence, radiance emitted by the Earth's surface and atmosphere. In the absence of diurnal variations, systematic differences in sampling time would not introduce systematic components of the overall uncertainty.

The selection of orbital data from GEO and LEO IR instruments is designed to select samples that are distributed with a uniform time difference between the limits specified in the

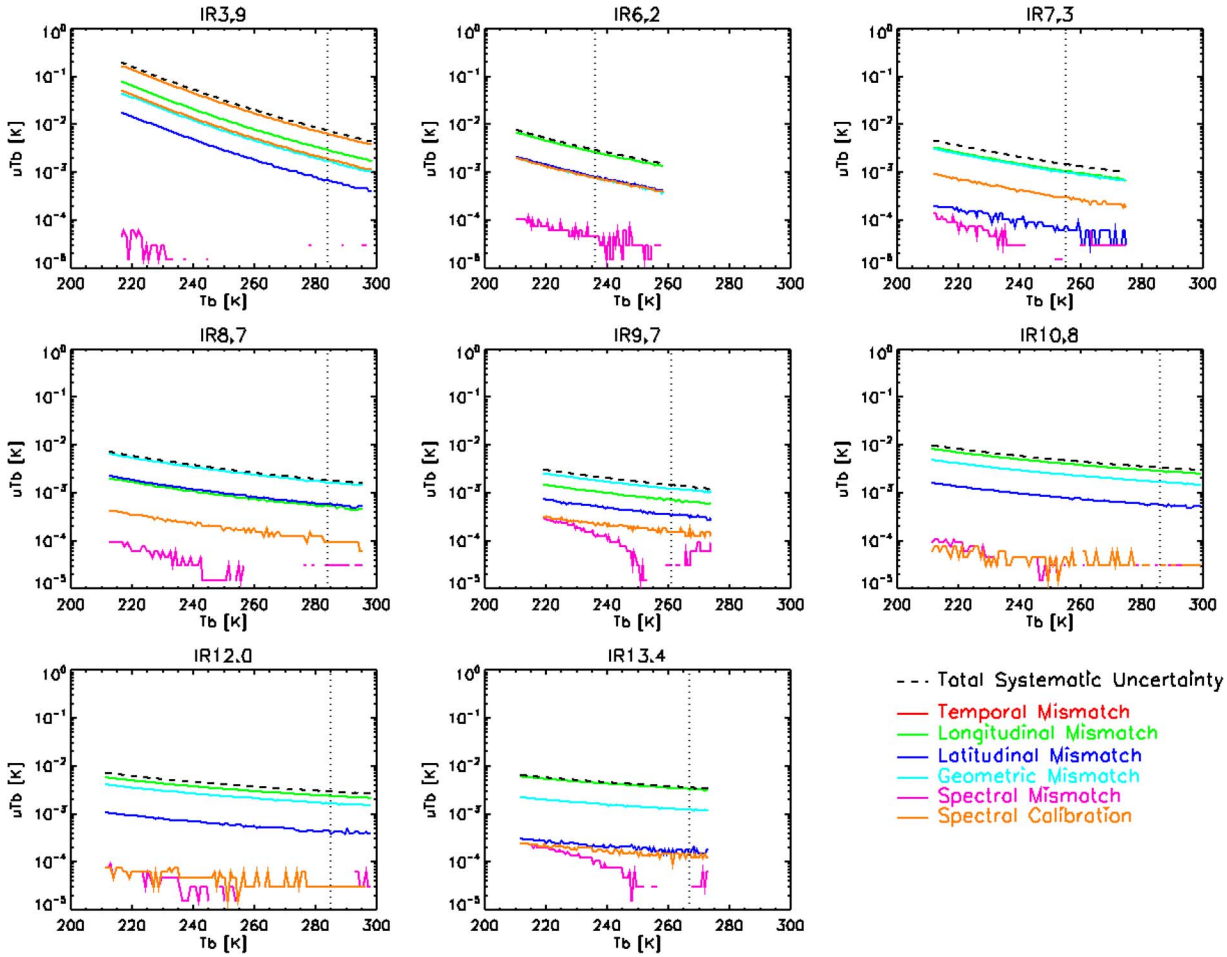

Fig. 1. Contribution of each source of systematic error $u_j^s(\hat{L})$ to the standard uncertainty of the brightness temperatures (Tb) produced by the GSICS correction for a range of scene radiances for each IR channel of Meteosat-9/SEVIRI using the Metop/IASI reference. The dotted vertical line shows the *standard radiance* for each channel, corresponding to nadir views of a calm ocean in clear standard atmosphere conditions.

collocation criteria ($\pm\Delta t_{\max} = 300$ s in this case). However, there is a mean difference between the times Meteosat and IASI observe the collocations of $\Delta t = 30$ s, assuming their clocks to be accurate. (For comparisons between older instruments with inaccurate clocks, this term could be much larger.) The sensitivity of the radiances to changes in sampling time $\partial L/\partial t^s$ has been evaluated by calculating the mean difference between a large ensemble of radiances observed by SEVIRI in successive images over the collocation target area 30° W $< x_i < 30^\circ$ E, 30° S $< y_j < 30^\circ$ N, near the Metop-A overpass time t_k =21:00–22:00 Coordinated Universal Time (UTC)

$$\left(\frac{\partial L}{\partial x^s}\right)_j = \frac{1}{n_i n_j n_k} \sum_{i,j,k} \left[L(x_i, y_j, t_k + \Delta t) - L(x_i, y_j, t_k)\right]. \tag{6}$$

Because only the data from the nighttime overpass of Metop-A are used in the intercalibration, the mean rate of change of surface temperature is relatively small (-0.2 K/h), so the radiances are relatively insensitive to systematic timing differences. Thus, temporal mismatches contribute < 0.01 K to the combined uncertainty of the SEVIRI radiances after applying the GSICS correction, as shown in Fig. 1.

C. Longitudinal and Latitudinal Mismatches

Systematic errors in the geolocation of both the monitored instrument and the reference instrument being compared introduce errors in their collocated radiances due to small longitudinal and latitudinal mean gradients in their radiances over the domain of the collocations.

As the exact geolocation error on each pixel is not known, we assume that they are distributed uniformly over the accuracies quoted for their navigation. The typical accuracy of the image navigation (rectification) for SEVIRI level 1.5 images based on the operational Image Processing Facility processing is calculated to be 1.2 km [11]. The geolocation accuracy of IASI level 1c data is calculated to be 1–2 km [12]. A value of 2 km is taken as a worst case limit. These errors are assumed to be partitioned equally between longitude and latitude. Their uncertainties are combined linearly to act as a guard band, so errors in longitudinal position are assumed to be distributed uniformly over $\pm\Delta\text{lon}_{\max} = (1.2 + 2)/\sqrt{2} = 2.26$ km. This is equivalent to a standard uncertainty of $\Delta\text{lon} = 2.26/\sqrt{3} = 1.30$ km. The sensitivity of the collocated radiances to systematic errors in longitude was calculated as the mean difference in radiances between adjacent pixels of a Meteosat-9 image over the target domain. Latitude geolocation errors are very similar to those

in longitude over most of the domain in which GEO–LEO collocations are generated. However, the radiances are more sensitive to errors in latitude than longitude, as expected, due to latitudinal temperature and humidity gradients.

It is interesting to note that, for most channels, the temporal mismatch is the dominant source of systematic uncertainty, whereas the latitudinal mismatch introduces larger uncertainty for the 8.7- and 9.7-μm channels. This may be due to latitudinal gradients of ice cloud and ozone to which these channels are sensitive.

D. Geometric Mismatch

Even if collocations are perfectly aligned in terms of surface location, observations from instruments on different satellites are never exactly aligned in terms of viewing and solar geometry. Although the radiances in the IR channels of SEVIRI are not sensitive to solar and azimuth angles during the nighttime conditions used in this study, they are affected by the incidence angle—both in terms of absorption along different atmospheric paths and changes in surface emissivity.

Pixels are defined as collocations only if their incidence angles are such that the ratio of their atmospheric path difference is less than 1% (i.e., $|\Delta \sec\theta / \sec\theta| < 0.01$). For a typical incidence angle $\theta = 30^\circ$, this corresponds to a difference $\Delta\theta = 1^\circ$. In practice, collocations may have different incidence angles uniformly distributed within the range $\pm\Delta\theta$. However, if the actual distribution of viewing-angle differences is not symmetric, systematic biases will be introduced into the intercalibration products. In this case, we can use the actual differences in *air mass*$(\sec\theta)$ calculated for the collocations used to generate a typical GSICS correction. These follow a rectangular distribution within the limits of $|\Delta \sec\theta / \sec\theta| < 0.01$, with a mean value of $\Delta \sec\theta / \sec\theta = -0.00069$.

The mean sensitivity to these changes was estimated by comparing the output of an RTM for each channel at incidence angles $\theta = 30^\circ$ and 29° over a range of atmospheric and surface conditions representing clear skies or uniform cloud at different heights.

Clouds introduce additional uncertainty due to parallax errors, the magnitude of which will depend on the geometry of each collocation (incidence angle θ and relative azimuth angle $\Delta\varphi$) as well as the cloud top height z_{CTH}. The uncertainty introduced by parallax errors can then be estimated using the sensitivities derived for spatial mismatches and variability, respectively, using a spatial offset of

$$\Delta x = \left\{2(z_{\mathrm{CTH}} \sin\theta)^2 (1 - \cos\Delta\varphi)\right\}^{1/2}. \tag{7}$$

The mean cloud top height over the area of collocations is estimated to be $z_{\mathrm{CTH}} = 2$ km (albeit with a large variance). For an incidence angle of $\theta = 30^\circ$, this introduces a mean parallax error of $\Delta x \sim 1.4$ km for the mean difference in GEO–LEO azimuth angle is $\Delta\varphi = 90^\circ$. This is comparable to the systematic uncertainty associated with one component of the geolocation (see *spatial mismatch* mentioned earlier) and the random uncertainty due to collocation (see *spatial variability* hereinafter). However, parallax errors will have a larger impact for collocations in areas of high cloud, which have much greater spatial variability and correspondingly produce higher uncertainty when applying the GSICS correction to low radiance scenes. This was confirmed experimentally by comparing the GSICS corrections calculated from collocations with low and high relative azimuth angles. The resulting differences were small, but just statistically significant in four of the eight channels, and were the largest for low radiance scenes.

E. Spectral Mismatch

When radiances measured with nonidentical channels are compared, great care must be taken to account for the differences introduced by their different spectral responses. Many methods have been developed to perform this *spectral correction*. However, no spectral correction method can be perfect, and residual errors will remain in the compared radiances, including systematic components. Even using a hyperspectral reference instrument, such as IASI, there are uncertainties introduced in the comparison of collocated radiances with a broadband radiometer, such as SEVIRI, due to the hyperspectral instrument's spectral calibration accuracy and gap-filling methods used to account for its incomplete spectral coverage of the GEO channels.

1) GEO–LEO Spectral Mismatch: Deficiencies in the hyperspectral reference instrument's coverage of the broadband monitored instrument need to be accounted for before their collocated observations can be compared. In the case of SEVIRI-IASI intercalibration, a simple approach can be adopted to account for this deficiency because only the IR3.9 channel of SEVIRI has incomplete coverage by IASI, which stops at 2760 cm^{-1}. The LBLRTM line-by-line code [13], with the HITRAN2004 spectroscopy line parameter database [14] including the Atmospheric and Environmental Research updates version 2.0 [15], was used to calculate radiance spectra over the full thermal IR range for nine atmospheres with different cloud amounts. These were convolved with the SEVIRI spectral response functions (SRFs) and the integral over the full band compared with the integral of those truncated at 2760 cm^{-1}. A simple linear model was developed to estimate the radiance over the full SRF from that integrated over the truncated SRF. This produced corrections ranging from -0.08 K to -0.35 K, depending on the scene radiance. The root mean square (rms) uncertainty on this correction for the IR3.9 channel was 0.005 K.

In general, there will also be contributions from the systematic errors in the RTM used to perform the spectral correction when comparing the observations of two instruments. However, in the case of SEVIRI-IASI, the uncertainty in the spectral correction is very small, so the modeling errors will have a negligible influence.

2) LEO Spectral Calibration Accuracy: Prelaunch characterization of IASI confirmed its channels' relative spectral shifts to be within the required limits of $\Delta\nu/\nu = 2$ ppm [12]. The sensitivity of the collocations' radiances to systematic shifts in the center frequency of the channels of IASI has been estimated by shifting the wavenumbers of the SRFs by this ratio and repeating the spectral convolution. The resulting radiances are negligibly different from those calculated for the unperturbed SEVIRI channels (< 1 mK).

3) GEO Spectral Calibration Accuracy: The official SRF of the channels of SEVIRI is calculated from a series of tests performed on their hardware components. These are combined and expressed at irregular wavelength intervals selected to represent the full SRF with minimal errors. However, the SRF definitions are open to interpretation, which may introduce errors in the radiances when compared to a hyperspectral reference instrument. For example, although it is recommended that a linear interpolation is used to convert the published SRFs to the IASI channel wavenumbers, it would be possible to use other interpolation methods. The calculations were repeated using linear and quadratic interpolations, and the results were compared to estimate the magnitude of likely errors introduced due to this ambiguity. This term is quite small ($\sim$0.01 K) and can be neglected if we assume that the SRFs are interpreted as recommended and in a consistent way in the application of the GEO observations and in the calculation of the intercalibration.

F. Combining and Comparing All Systematic Errors

All the uncertainties due to systematic processes j are added in quadrature to give the total $u^s(\hat{L})$

$$u^s(\hat{L}) = \left\{ \sum_j \left(u_j^s(\hat{L}) \right)^2 \right\}^{1/2}. \tag{8}$$

This total uncertainty on the corrected radiance due to all systematic errors is compared with the contribution from each considered mechanism in Fig. 1. Here, the uncertainties have been evaluated for the range of radiances observed over all the collocations used in the sample case. The full dynamic range of SEVIRI can be somewhat larger but would require many more cases to generate reliable statistics to cover.

The radiances and uncertainties are converted to brightness temperatures for convenient comparison. This causes the uncertainties for low scene radiances to appear larger, due to the nonlinearity of the Planck function. Although this contributes to the uncertainties for low scene radiances appearing larger, this increase is mostly due to the distribution of collocated radiances used in the regression and their weights. Thus, the lowest uncertainties are found for the most popular radiances in the distribution, which also have the lowest variance as they correspond to clear sky scenes. This minimum uncertainty also happens to occur close to the standard radiance scene in most cases—although the standard radiances are lower than the modal values for water vapor channels (IR6.2 and IR7.3), due to the U.S. standard atmosphere being drier than the typical values found in the collocations' tropical domain.

Fig. 1 shows that the total systematic uncertainty is generally dominated by systematic mismatches in time and space due to finite gradients in the scene over the intercalibration target domain. However, as noted previously, parallax errors are likely to have an impact that is at least comparable to the navigation mismatches. Furthermore, these would be much larger (up to a factor of ten) if daytime collocations were used instead of only nighttime ones, due to stronger spatial and temporal gradients.

However, the systematic errors in the IR3.9 channel are dominated by the uncertainty in the spectral correction method applied to compensate for the incomplete coverage of this channel by IASI. Other terms due to geometric mismatches and the spectral calibration of the reference instrument are negligible in all cases and appear erratic due to the limitations of numerical precision.

Furthermore, these results suggest that the specified collocation criteria for the difference of viewing zenith angle $|\Delta \sec\theta / \sec\theta| < 0.01$ could be substantially relaxed without causing a significant increase in the combined uncertainty of the intercalibration result. However, subsequent trials with a relaxed threshold resulted in an increase in the time series variance of the standard biases—perhaps due to the underaccounted influence of cloud parallax errors.

IV. Random Errors

Various processes can also introduce random errors on each collocated radiance. The magnitude of these can be estimated from the typical range of each variable and the sensitivity of the radiances to perturbations of each variable, which again can be derived from a statistical analysis of case studies.

A. Methodology for Random Errors

A Monte Carlo approach is adopted to evaluate the uncertainty on the final GSICS correction due to processes which introduce random errors. The radiance of each collocated point is perturbed by an uncertainty calculated by multiplying a random number z_i drawn from a distribution consistent with a characteristic difference Δx^r multiplied by the sensitivity to random perturbations of each process j, $(\partial L/\partial x^r)_j$, as follows:

$$u_j^r(L_i) = z_i \overline{\Delta x_j^r} \left(\frac{\partial L}{\partial x^r} \right)_j. \tag{9}$$

Table II summarizes the magnitude of typical perturbations Δx_j of processes introducing random errors in the collocated radiances and the sensitivity of the IR channels of SEVIRI to these perturbations $\partial L/\partial x^r$. The origins of these values are discussed in the following sections.

The regression used to calculate the GSICS correction is then re-evaluated with one set of randomly perturbed radiances. The resulting regression coefficients are used to evaluate the bias over a range of scene radiances. This procedure is then repeated a large number $(n_k = 100)$ of times to give n_k evaluations of $g_{j,k}^r(L)$. Each evaluation of which is used to calculate a corrected radiance for each of a range of scene radiances $\hat{L}'_{j,k}$. The standard deviation of $\hat{L}'_{j,k}$ over the Monte Carlo ensemble is then calculated to estimate the uncertainty on corrected radiances due to each random process j, which are shown in Fig. 2

$$u_j^r(\hat{L}) = \left\{ \frac{1}{n_k - 1} \sum_{k=1}^{n_k} \left(g_{j,k}^r(L) - g_j(L) \right)^2 \right\}^{\frac{1}{2}}. \tag{10}$$

TABLE II
SUMMARY OF THE RANDOM ERRORS' PERTURBATIONS AND SENSITIVITIES TO EACH COLLOCATED RADIANCE

Random Error Type	Δx_j^r		*Sensitivity,* $\partial L_j/\partial x^r$ [$\mu W/m^2/sr/cm^{-1}/\Delta x$]							
			IR3.9	IR6.2	IR7.3	IR8.7	IR9.7	IR10.8	IR12.0	IR13.4
Temporal Variability	300	s	0.045	0.096	0.551	2.774	1.921	4.178	4.434	2.807
Longitudinal Variability	3.411	km	4.11	6.91	40.7	232.4	157.3	340.5	354.3	211.6
Latitudinal Variability	3.381	km	4.48	8.08	47.4	259.9	177.3	385.3	403.5	244.8
Geometric Variability	1		0.49	8.6	30.6	34.6	109.9	37.4	47.8	112.8
Spectral Variability	1		0.14	0	0	0	0	0	0	0
Radiometric Noise (GEO)	1		0.54	1.7	5.9	25.5	28.1	32.7	48.2	94.0
Radiometric Noise (LEO)	1		0.76	1.2	2.1	28.7	29.1	23.7	28.0	24.9

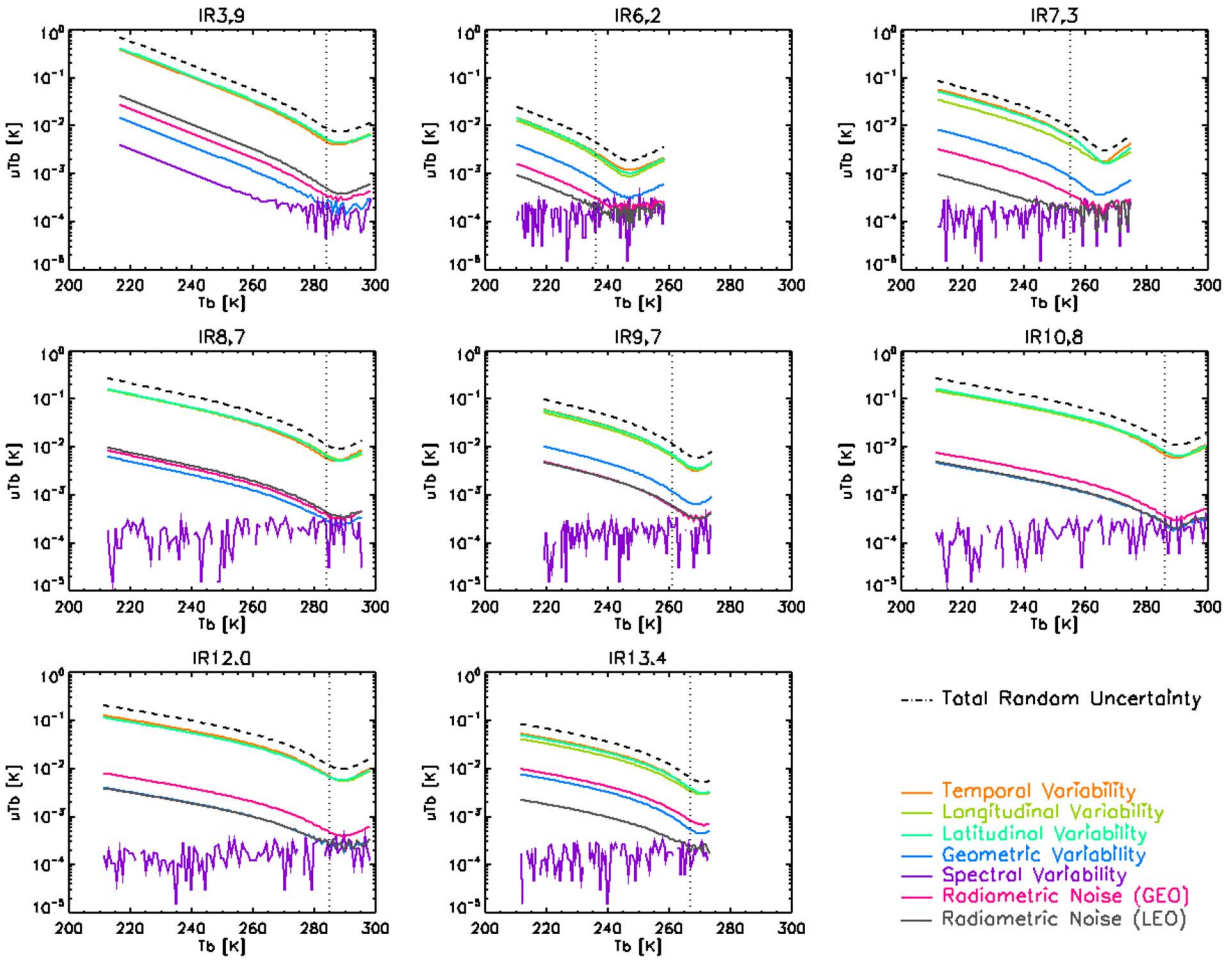

Fig. 2. Contribution of each source of random error $u_j^r(\hat{L})$ to the standard uncertainty of the brightness temperatures (Tb) produced by the GSICS correction for a range of scene radiances for each IR channel of Meteosat-9/SEVIRI using the Metop/IASI reference. The dotted vertical line shows the *standard radiance* for each channel, corresponding to nadir views of a calm ocean in clear standard atmosphere conditions.

B. Temporal Variability

Collocated observations from a pair of satellite instruments are not sampled exactly simultaneously. Variations in the atmosphere and surface during the interval between their observations introduce errors when comparing their collocated radiances. The greater this interval, the larger the contribution of the scene's temporal variability to the total error budget. The uncertainty that this introduces to the collocated radiances can be quantified by statistical analysis of a series of SEVIRI scenes described hereinafter.

GEO imagers sample scenes at regular intervals: SEVIRI can scan the whole Earth disk every 15 min or one-third of it every 5 min in rapid scan mode. The latter corresponds to the maximum interval recommended in the ATBD for its pixels to be considered collocated with those of IASI [4]. This finite sampling introduces a temporal collocation error with a uniform distribution over $\pm\Delta t_{\max} = 300$ s. This is equivalent to an rms difference between sampling of SEVIRI and IASI observations of $\Delta t = \Delta t_{\max}/\sqrt{3} \approx 173$ s.

The temporal variability of typical SEVIRI images is quantified for each IR channel in the Appendix. Variograms were calculated as the rms difference of each channel's radiances in pairs of images sampled in rapid scanning mode at various intervals. This analysis suggests that the 5-min collocation

threshold introduces random uncertainties of 1 K–2 K in the window channels and much less in the water vapor channels. These variograms are used here to estimate the sensitivity of the radiances to differences in sampling time $\partial L/\partial t$.

C. Longitudinal and Latitudinal Variability

Similarly, collocated observations from a pair of satellite instruments are not exactly collocated, and spatial variations in the atmosphere and surface introduce errors when comparing their collocated radiances. The greater the separation between their observations, the larger the contribution of the scene's spatial variability to the total error budget. The uncertainty that this introduces to the collocated radiances is quantified by statistical analysis of representative SEVIRI scenes as follows.

The level 1.5 data of SEVIRI have been reprojected onto a grid, with approximately uniform spacing near the subsatellite point and over the target domain of the collocations, where the median distances between adjacent pixels are $\Delta\text{lon}_{\max} = 3.41$ km and $\Delta\text{lat}_{\max} = 3.38$ km. Because this is greater than the random part of the uncertainty in the geolocation of either instrument, their collocations are assumed to follow uniform distributions over $\pm\Delta\text{lon}_{\max}$ and $\pm\Delta\text{lat}_{\max}$.

Even if a GEO satellite instrument did not reproject its pixels onto a fixed grid, there would still be a random contribution to the uncertainty due to spatial variability, because geolocation differences between the GEO and LEO instruments would introduce sensitivity to the scene's spatial variability.

The spatial variability of a typical SEVIRI image is also quantified for each IR channel in the Appendix. Variograms were calculated as the rms difference of each channel's radiances after shifting the images by various latitude and longitude offsets. This analysis suggests that the 3.5-km effective collocation threshold introduces random uncertainties of 1 K–2 K in the window channels and much less in the water vapor channels. These variograms are used here to estimate the sensitivity of the radiances to differences in spatial sampling $\partial L/\partial\text{lon}$ and $\partial L/\partial\text{lat}$.

D. Geometric Variability

Random differences between the viewing and solar geometry of the collocations observed by the monitored and reference instruments also introduce random errors to their collocated radiances. As in the case of the systematic geometric mismatches (above), the differences in viewing zenith angle between the two sensors are uniformly distributed within a range corresponding to a $< 1\%$ difference in atmospheric path. Likewise, the sensitivity of the collocated radiances to viewing zenith angle is the same as for systematic geometric mismatches.

As previously mentioned, cloud can introduce parallax errors, including some random components, which could be modeled as an increased random uncertainty in relative geolocation of the collocated pixels. As in the case of the systematic components of cloud parallax errors, these are expected to have a mean contribution to uncertainty equivalent to the spatial variability on a scale of $\Delta x \sim 1.4$ km, which is small relative to spatial variability. However, the equivalent perturbation should be more accurately modeled as a function of scene radiance, and in the case of high cloud, parallax errors will further increase the uncertainty, which warrants further investigation for applications concerned with low radiance scenes.

E. Spectral Variability

Although IASI spectral calibration errors are expected to be systematic, the same magnitudes and sensitivities are used here to investigate the impact of random spectral errors, assuming that they follow a normal distribution with $\Delta\nu/\nu = 2$ ppm. As this analysis shows this term to have a negligible contribution to the random component of the uncertainty on collocated radiances, this approximation is not further elaborated upon.

F. Radiometric Noise

All radiometer observations suffer from radiometric noise caused by limitations of the instruments. This noise, which is assumed to be white, contributes to the uncertainty in the comparison of collocated observations. However, the impact of radiometric noise is reduced by averaging multiple observations, spatially, temporally, and spectrally. Furthermore, these terms are implicitly included in both the spatial and temporal variability terms as calculated earlier, as they use real observational data, which include radiometric noise. It is, therefore, reassuring to see from Fig. 2 that these terms have negligible contributions to the combined uncertainties. So, although they have been double counted in the error budget, this does not matter as their contributions are insignificant compared to the temporal and spatial variability of the scene.

G. Combining and Comparing All Random Errors

All the uncertainties due to random processes j are added in quadrature to give $u^r(\hat{L})$

$$u^r(\hat{L}) = \left\{ \sum_j \left(u_j^r(\hat{L}) \right)^2 \right\}^{1/2}. \tag{11}$$

This total uncertainty on the corrected radiance due to all random errors is compared with the contribution from each considered mechanism in Fig. 2. Here, the uncertainties have been evaluated for the range of radiances observed over all the collocations. The radiances and their uncertainties are converted to brightness temperatures for convenient comparison.

Fig. 2 shows that the random variability in time and space dominates the total random uncertainty in all channels. As for the systematic components of the uncertainty, the random components increase rapidly as the scene radiance decreases. However, this increase may be underestimated by the method of applying the same magnitude perturbation and sensitivity to all scene radiances, whereas in reality, the scene variability and parallax errors tend to increase when cold cloud is present in the collocation scene.

Other terms due to geometric and spectral variability are negligible in all cases, and the latter appear erratic due to

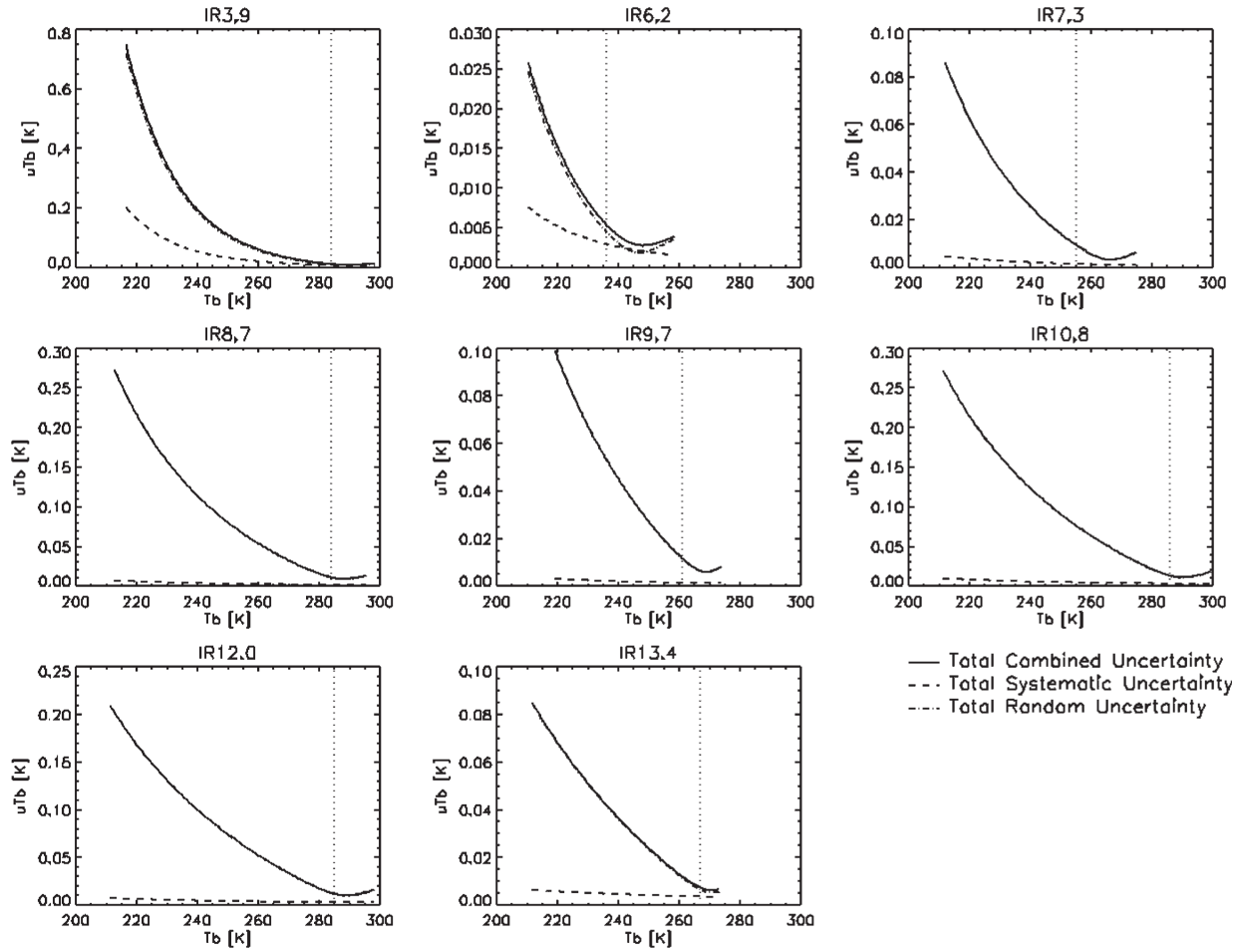

Fig. 3. Impact of total systematic $u^s(\hat{L})$, random $u^r(\hat{L})$, and combined $u^c(\hat{L})$ errors on $(k = 1)$ uncertainty of the brightness temperatures (Tb) produced by the GSICS correction for a range of scene radiances for each IR channel of Meteosat-9/SEVIRI using the IASI reference. The dotted vertical line shows the *standard radiance* for each channel.

the limitations of numerical precision. These results suggest that the time limit of $|\Delta t| < 300$ s specified in the collocation criteria is well matched to the spatial variability due to the 3-km sampling of SEVIRI.

V. Combining Systematic and Random Errors

A. Method for Combining Systematic and Random Errors

The total uncertainties due to systematic and random processes can then be combined to give the total combined uncertainty u^c for a given radiance $\hat{L}$

$$u^c(\hat{L}) = \left\{ \left[u^s(\hat{L})\right]^2 + \left[u^r(\hat{L})\right]^2 \right\}^{1/2}. \tag{12}$$

Fig. 3 compares the impacts of the total systematic and random errors on the uncertainty of the GSICS correction evaluated over a range of scene radiances. This shows that, in most conditions, the random components of the uncertainty dominate for all channels. These uncertainties are much smaller for channels with stronger atmospheric absorption, as the scenes are inherently less variable. Fig. 3 also shows that the uncertainties increase rapidly for low radiance scenes and reach a minimum near the standard radiances for each channel. This is because the majority of the collocations give radiances near these values, whereas cold high clouds, which give low radiances, are relatively infrequent and more variable.

Here, the uncertainties on the GSICS correction have been evaluated for typical sets of collocations used to calculate the *reanalysis correction*. In general, the random components of the uncertainty would scale as the inverse square of the number of collocations $n^{-1/2}$, assuming them to be independent. So, the random components of the uncertainty of the *near-real-time corrections* would be a factor of $\sqrt{2}$ larger due to approximately half the number of collocations being used in the regression. However, the systematic components of the uncertainty are independent of the sample size.

B. Validation of Quoted Uncertainty on GSICS Correction and Theory

There are inevitably always sources of uncertainty that are omitted from such analyses. Hence, there is a need for validation, which is possible for the random components, at least. Table III compares the total uncertainty due to random errors predicted by this analysis with the median value of the uncertainty quoted within the demonstration GSICS reanalysis products evaluated over 2010. This shows that the regression

TABLE III
OVERALL ERROR BUDGET OF GSICS CORRECTION FOR SEVIRI-IASI AND VALIDATION OF RANDOM COMPONENT (ALL UNCERTAINTIES ARE $k = 1$)

Meteosat/ SEVIRI Channel	*IR3.9*	*IR6.2*	*IR7.3*	*IR8.7*	*IR9.7*	*IR10.8*	*IR12.0*	*IR13.4*	*Unit*
Standard Radiance (as Tb)	284	236	255	284	261	286	285	267	K
Typical Standard Correction	0.071	-0.130	0.204	-0.002	-0.048	0.002	0.095	-1.136	K
Total Random Uncertainty from this analysis	0.009	0.004	0.009	0.011	0.012	0.013	0.011	0.006	K
Median Quoted Uncertainty from ATBD	0.004	0.004	0.004	0.003	0.006	0.003	0.004	0.006	K
Rolling SD of Standard Bias from observations	0.013	0.016	0.017	0.022	0.022	0.020	0.016	0.021	K
Total Systematic Uncertainty	0.008	0.003	0.002	0.002	0.002	0.003	0.003	0.004	K
Total Combined Uncertainty	0.012	0.005	0.009	0.012	0.012	0.013	0.012	0.007	K

used in the ATBD tends to underestimate the uncertainties by a factor which ranges from one to four.

Table III also compares the results of this analysis with the day-to-day variability observed in the biases estimated for standard radiance scenes, calculated as the median rolling standard deviation over 15-day windows. These show that the GSICS correction gives more variable results than expected by considering only the random processes affecting the intercalibration process. This difference between the theoretical uncertainty and the observed day-to-day variability is partly due not only to the underestimation of parallax error but also to real variations in the instruments' calibration, which may be of the same order as the uncertainties evaluated here.

Also shown in Table III are the systematic, random, and combined uncertainties of the *GSICS reanalysis correction* for standard radiance scenes. These values are generally small, with total combined standard uncertainties of $\sim$10 mK. These can be compared to typical corrections for standard radiances for each channel, which are generally an order of magnitude larger. This shows that, although the corrections are small, they are statistically significant at the 95% level for all channels except IR8.7 and IR10.8.

VI. CONCLUSION

Like all calibrations, the GEO–LEO GSICS correction for the IR channels of Meteosat/SEVIRI, which uses Metop/IASI as a reference, should include stated uncertainties, to provide traceability and allow users to judge the confidence that they can put in the resulting radiances and in other products derived from them. This paper has evaluated the uncertainties for the *reanalysis* version of this GSICS correction when SEVIRI is operating in the normal full-disk scanning mode. It shows that random errors dominate systematic ones and that combined standard uncertainties (i.e., with coverage factor $k = 1$) in the corrected brightness temperatures are $\sim$0.01 K for typical clear sky conditions. However, this analysis suggests that uncertainties increase rapidly for low radiances—by more than one order of magnitude for scenes of 210 K, corresponding to deep convective cloud tops. This is not only due to there being fewer collocations with low radiances but also their greater variability, which is used as a weighting in the regression. However, in reality, the GSICS corrections' uncertainty for cold scenes would be further increased due to parallax errors, which have not been fully accounted for in this analysis and would require the uncertainty on each collocation to be modeled as a function of scene radiance and geometry. This is the subject for future work, following the iterative procedure for uncertainty management [10].

These random errors are dominated by spatial and temporal variability of the scene within the collocations, even though their effects are reduced by the large number of collocations. In the contrasting case of polar simultaneous nadir overpasses often used to intercalibrate LEO–LEO sensors, the spatial and temporal variability would be proportionally larger, because the number of collocations is much smaller. Similarly, the random components of the GEO–LEO *near-real-time corrections* would be a factor of $\sqrt{2}$ larger due to approximately half the number of collocations being used in the regression. Systematic errors would remain largely unchanged.

Ideally, the intercalibration algorithm would include a full error propagation, evaluated dynamically. As this is a relatively cumbersome process, it has been simplified by considering the dominant sources of uncertainty: random variability in space—and time, by proxy. However, this analysis shows that this simplified treatment of uncertainty in the ATBD [6] results in an underestimation of the uncertainty. It is therefore recommended that values quoted within the current intercalibration products are inflated by a factor of approximately two to achieve greater consistency between the statistics of the GSICS correction and this analysis.

This analysis does not include contributions associated with the interpretation of the SRFs published for the GEO imager, which could dominate the systematic errors of most channels if included. This highlights the importance of communicating clear guidance in the application of published SRFs.

Although some of these recommendations can be generalized to other pairs of GEO–LEO hyperspectral IR intercalibrations, the analysis should be repeated for each intercalibration product. Particular attention should be paid to the analysis of any *gap-filling* methods used in spectral corrections, which could dominate the uncertainties for other products which do not use hyperspectral instruments with continuous spectral coverage, such as IASI, as a reference. This uncertainty analysis can be extended to similar intercalibration problems. In general, if the desired uncertainty in the final intercalibration product is first established, it would be possible to estimate the sample size necessary to reduce the uncertainties from spatial and temporal scene variability to the required level and therefore determine the frequency at which the intercalibration can be updated.

APPENDIX
QUANTIFYING SCENE VARIABILITY

The intercalibration of satellite instruments often requires comparing observations from different instruments coincident in space, time, and viewing geometry. As these are never exact, thresholds are usually applied to define the collocations. The choice of these thresholds directly impacts the uncertainty of the comparison, partially due to the scene variability within the range of the collocation criteria. The collocation criteria represent tradeoffs between the errors on each collocation and the number of collocations available.

Scene variability can be quantified as a *variogram* by evaluating the rms difference of a series of observations sampled at different intervals in space or time [16]. Variograms are also known as empirical semivariances and are similar to the concept of *structure functions* in meteorology [17] and Allan variance [18]. They allow the variability of stochastic processes to be quantified over specific spatial or temporal scales and can quantify errors of representativeness in the use of satellite data. Variograms are evaluated here using data from the IR channels of the Meteosat/SEVIRI GEO imager.

A. Temporal Variability

The temporal variogram $2\gamma_t(\Delta t)$ is calculated between brightness temperatures $T_b s$ sampled at different intervals Δt from an extended time series $T_b(t)$

$$2\hat{\gamma}_t(\Delta t) := \frac{1}{n_i n_j n_k} \times \sum_{i,j,k} \left[T_b(x_i, y_j, t_k + \Delta t) - T_b(x_i, y_j, t_k)\right]^2 \quad \text{(A1)}$$

where x_i and y_j are the longitude and latitude over the SEVIRI grid, respectively, and t_k represents a time series of SEVIRI images.

Here, the Tb variability is estimated from observations from the IR channels of the Meteosat-8/SEVIRI imager, which provides data sampled every 3 km at nadir and every 15 min in normal operations over the full Earth disk (or every 5 min over a limited area). The red curve in Fig. 4 shows $2\gamma_t(\Delta t)$ for the 10.8-μm channel on temporal scales of $\Delta t = 5$ min to 16 h.

This temporal variogram was calculated from a series of observations made in rapid scanning mode on April 18, 2008, sampling the area 15° N 30° W−30° E, 45° N 45° W−45° E, every 5 min over a 24-h period. The results are similar to those calculated from a larger area (within 30° latitude/longitude of the subsatellite point) scanned every 15 min over a different 24-h period (February 4, 2006).

The temporal variogram, shown as the red curve in Fig. 4, shows the temporal variability peaks at $\Delta t \sim 12$ h, corresponding to the diurnal cycle. This is common to all channels, but most pronounced in the window channels. It is apparent that the diurnal cycle dominates variability on time scales longer than ∼1 h, causing γ_t to increase more rapidly for increasing time intervals.

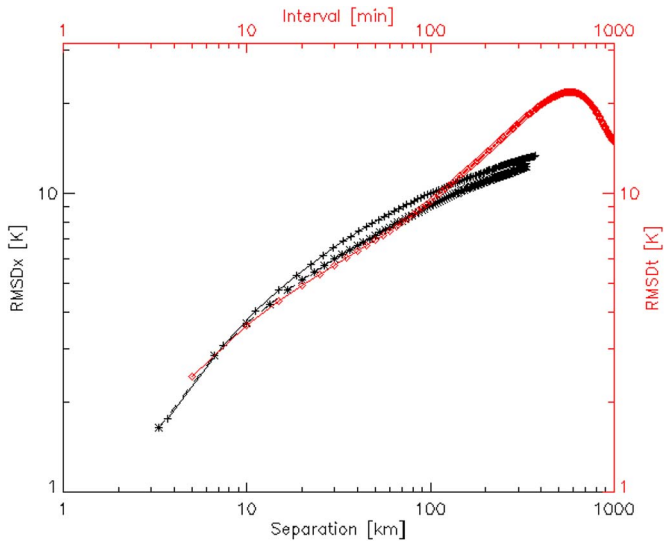

Fig. 4. Variograms calculated as rms differences in Meteosat-8/SEVIRI 10.8-μm brightness temperatures (red diamonds, upper x-axis) with time intervals from rapid scanning data and with spatial separation in (black pluses, lower x-axis) the north–south direction and (black stars, lower x-axis) the west–east direction.

B. Spatial Variability

The spatial T_b variability was calculated over the area within 30° latitude/longitude of the subsatellite point from the data obtained at February 1, 2006, 01:00 UTC. The image in each channel was shifted by variable distances Δx, and the spatial variogram γ_x was calculated for each as

$$2\hat{\gamma}_x(\Delta x) := \frac{1}{n_i n_j n_k} \times \sum_{i,j,k} \left[T_b(x_i + \Delta x, y_j, t_k) - T_b(x_i, y_j, t_k)\right]^2. \quad \text{(A2)}$$

As expected, the black curves in Fig. 4 show that the γ_x increases with increasing spatial separation at scales $\Delta x = 3$ to 1000 km. There is more T_b variability in the north/south direction than the east/west direction because of the global latitudinal temperature gradient. However, this difference becomes negligible on scales smaller than ∼10 km.

C. Matching Spatial and Temporal Collocation Criteria

This method allows the scene variability to be quantified for observations sampled at any interval in space or time. For example, Table IV shows the spatial and temporal variograms evaluated as the rms difference in scene $T_b s$ sampled every 3.5 km and 5 min, respectively. For all channels, $\gamma_t(\Delta t = 5 \text{ min})$ and $\gamma_x(\Delta x = 3.5 \text{ km})$ were found to produce similar variances. Therefore, in the case of SEVIRI, the random component of uncertainty in each collocation due to scene variability can be estimated by scaling the observed spatial variability alone by a factor of $\sim \sqrt{2}$.

D. Filtering

A homogeneity filter can be applied by excluding pixels where the standard deviation of radiances within 5 × 5 pixels

TABLE IV
TEMPORAL AND SPATIAL VARIOGRAMS EVALUATED AS RMS DIFFERENCE OF METEOSAT-8 BRIGHTNESS TEMPERATURES ON SCALES OF 5 min AND 3.5 km, RESPECTIVELY

Channel [μm]	$\{2\gamma_t(\Delta t{=}5\text{min})\}^{1/2}$ [K]	$\{2\gamma_x(\Delta x{=}3.5\text{km})\}^{1/2}$ [K]
3.9	1.7	2.1
6.2	0.4	0.5
7.3	0.8	0.8
8.7	1.7	1.6
9.7	0.9	1.2
10.8	1.8	1.7
12.0	1.8	1.6
13.4	1.2	1.2

is $> 5\%$ of the mean radiance. When this is applied prior to the calculation, γ_t drops by a factor of 2.0, and γ_x reduces by a factor of 2.6. Selecting only clear sky cases will further reduce both γ_t and γ_x. On very small scales, or for homogeneous scenes, the atmospheric variability becomes negligible compared to the instrument's radiometric noise, and γ_x and γ_t become constant with space and time, respectively.

E. Conclusion

In this paper, the optimization of collocation thresholds has been found to depend on how much noise is acceptable to introduce into each collocation due to scene variability. For example, these results suggest that thresholds of 5 min and 3.5 km would each introduce random uncertainties of about 1 K–2 K into each collocation for window channels (and much less for water vapor channels). These may be reduced to insignificant levels if many independent collocations are combined in the analysis. However, adjacent collocations are highly correlated (autocorrelation $1/e$ scales are about 600 km and 6 h), so it is not trivial to optimize the collocation thresholds from this analysis alone.

ACKNOWLEDGMENT

The author would like to thank R. Kessel (currently at the Physikalisch-Technische Bundesanstalt) for his valuable advice on the method used in this analysis during the author's time as a Visiting Scientist at the European Organisation for the Exploitation of Meteorological Satellites, while working for the National Institute of Standards and Technology, and the anonymous reviewers for the comments and advice that helped in improving this paper.

REFERENCES

[1] M. Goldberg, G. Ohring, J. Butler, C. Cao, R. Datla, D. Doelling, V. Gaertner, T. Hewison, B. Iacovazzi, D. Kim, T. Kurino, J. Lafeuille, P. Minnis, D. Renaut, J. Schmetz, D. Tobin, L. Wang, F. Weng, X. Wu, F. Yu, P. Zhang, and T. Zhu, "The Global Space-based Inter-Calibration System (GSICS)," *Bull. Amer. Meteorol. Soc.*, vol. 92, no. 4, pp. 467–475, Apr. 2011.

[2] G. Chander, D. L. Helder, D. Aaron, N. Mishra, and A. Shrestha, "Assessment of spectral, misregistration, and spatial uncertainties inherent in the cross-calibration study," *IEEE Trans. Geosci. Remote Sens.*, vol. 51, no. 3, pp. 1282–1296, Mar. 2013.

[3] T. Chang and X. Xiong, "Assessment of MODIS thermal emissive bands on-orbit calibration," *IEEE Trans. Geosci Remote Sens.*, vol. 49, no. 6, pp. 2415–2425, Jun. 2011.

[4] T. J. Hewison, X. Wu, F. Yu, Y. Tahara, X. Hu, D. Kim, and M. Koenig, "GSICS inter-calibration of infrared channels of geostationary imagers using Metop/IASI," *IEEE Trans. Geosci. Remote Sens.*, vol. 51, no. 3, pp. 1160–1170, Mar. 2013.

[5] X. Wu, T. Hewison, and Y. Tahara, "GSICS GEO–LEO intercalibration: Baseline algorithm and early results," presented at the Proc. SPIE Optics Photonics, San Diego, CA, Aug. 5, 2009, Paper 7456-3.

[6] T. Hewison, ATBD for EUMETSAT's inter-calibration of SEVIRI-IASI, EUMETSAT, Darmstadt, Germany, Rep. EUM/MET/REP/08/0468. [Online]. Available: http://www.eumetsat.int/groups/ops/documents/document/PDF_ATBD_GSICS_SEVIRI_IASI.pdf

[7] *Evaluation of Measurement Data—Guide to the Expression of Uncertainty in Measurement*, Bur. Int. des Poids et Mesures, Sèvres, France, 2008, Joint Committee for Guides in Metrology, JCGM 100:2008.

[8] N. Fox, "A guide to expression of uncertainty of measurements," Group Earth Observ., Geneva, Switzerland, QA4EO-QAEO-GEN-DQK-006, 2010, QA4EO Guideline.

[9] *Geometrical Product Specifications (GPS)—Inspection by Measurement of Workpieces and Measuring Equipment—Part 2: Guidance for the Estimation of Uncertainty in GPS Measurement, in Calibration of Measuring Equipment and in Product Verification*, ISO 14253-2:2011.

[10] S. Nuccio and C. Spataro, "Uncertainty management in the measurements performed by means of virtual instruments," in *Proc. IEEE Int. Workshop AMUEM*, Jul. 21/22, 2008, pp. 40–45.

[11] *Typical Geometrical Accuracy for MSG-1/2*, EUMETSAT, Darmstadt Germany, 2007, EUMETSAT Report EUM/OPS/TEN/07/0313.

[12] D. Blumstein, G. Chalon, T. Carlier, C. Buil, P. Hebert, T. Maciaszek, G. Ponce, T. Phulpin, B. Tournier, D. Simeoni, P. Astruc, A. Clauss, G. Kayal, and R. Jegou, "IASI instrument: Technical overview and measured performances," in *Proc. SPIE*, 2004, vol. 5543, pp. 196–207.

[13] S. A. Clough and M. J. Iacono, "Line-by-line calculations of atmospheric fluxes and cooling rates II: Application to carbon dioxide, ozone, methane, nitrous oxide, and the halocarbons," *J. Geophys. Res.*, vol. 100, no. D8, pp. 16 519–16 535, Jan. 1995.

[14] L. S. Rothman, A. Barbe, D. C. Benner, L. R. Brown, C. Camy-Peyret, M. R. Carleer, K. Chance, C. Clerbaux, V. Dana, V. M. Devi, A. Fayt, J.-M. Flaud, R. R. Gamache, A. Goldman, D. Jacquemart, K. W. Jucks, W. J. Lafferty, J.-Y. Mandin, S. T. Massie, V. Nemtchinov, D. A. Newnham, A. Perrin, C. P. Rinsland, J. Schroeder, K. M. Smith, M. A. H. Smith, K. Tang, R. A. Toth, J. V. Auwera, P. Varanasi, and K. Yoshino, "The HITRAN molecular spectroscopic database: Edition of 2000 including updates through 2001," *J. Quant. Spectrosc. Radiat. Transf.*, vol. 82, no. 1–4, pp. 5–44, Nov./Dec. 2003.

[15] Atmospheric and Environmental Research (AER), Inc., AER's Radiative Transfer Working Group . [Online]. Available: http://rtweb.aer.com/main.html, AER's Radiative Transfer Working Group

[16] N. Cressie, *Statistics for Spatial Data*. New York: Wiley, 1993.

[17] M. Kitchen, "Representativeness errors for radiosonde observations," *Q.J.R. Meteorol. Soc.*, vol. 115, no. 487, pp. 673–700, Apr. 1989.

[18] D. W. Allan, "Statistics of atomic frequency standard," *Proc IEEE*, vol. 54, no. 2, pp. 221–230, Feb. 1996.

Tim J. Hewison (M'96–SM'13) received the Ph.D. degree in meteorology from the University of Reading, Reading, U.K., in 2006, based on his thesis on the use of ground-based microwave radiometers for atmospheric temperature and humidity profiling.

He is currently a Meteorological Scientist at EUMETSAT, Darmstadt, Germany, concentrating on the calibration of current, past and future satellite instruments. He also currently chairs the Research Working Group of the Global Space-based Inter-Calibration System (GSICS).